

The 193 (and 248) nm photolysis of HN₃: Formation and internal energy distributions of the NH (a 1 Δ , b 1 Σ^+ , A 3 Π , and c 1 Π) states

F. Rohrer and F. Stuhl

Citation: *The Journal of Chemical Physics* **88**, 4788 (1988); doi: 10.1063/1.454691

View online: <http://dx.doi.org/10.1063/1.454691>

View Table of Contents: <http://scitation.aip.org/content/aip/journal/jcp/88/8?ver=pdfcov>

Published by the [AIP Publishing](#)

Articles you may be interested in

[Vibrational distributions of NH \(a 1 \$\Delta\$ \) from the photolysis of HN₃ from 220–290 nm](#)

J. Chem. Phys. **99**, 2638 (1993); 10.1063/1.465226

[Energy partitioning in the 266 nm dissociation of HN₃ and relative transition probabilities in the NH \(c 1 \$\Pi\$ ↔a 1 \$\Delta\$ \) system](#)

J. Chem. Phys. **93**, 8777 (1990); 10.1063/1.459266

[Photodissociation of RNCS and RSCN \(R=H, CH₃, C₂H₅\) at 248 and 193 nm: CN product energy distributions](#)

J. Chem. Phys. **93**, 2346 (1990); 10.1063/1.459014

[Generation of NH\(a 1 \$\Delta\$ \) in the 193 nm photolysis of ammonia](#)

J. Chem. Phys. **86**, 2036 (1987); 10.1063/1.452153

[Formation of NH\(c 1 \$\Pi\$ \) and NH\(A 3 \$\Pi\$ \) in the Vacuumuv Photolysis of HN₃](#)

J. Chem. Phys. **45**, 4373 (1966); 10.1063/1.1727513



The 193 (and 248) nm photolysis of HN_3 : Formation and internal energy distributions of the $\text{NH}(a\ ^1\Delta, b\ ^1\Sigma^+, A\ ^3\Pi, \text{ and } c\ ^1\Pi)$ states

F. Rohrer^{a)} and F. Stuhl

Physikalische Chemie I, Ruhr-Universität, D-4630 Bochum, Federal Republic of Germany

(Received 9 November 1987; accepted 23 December 1987)

The UV photolysis of HN_3 at 193 nm was investigated in detail in the bulk phase at 300 K. NH radicals in the $X, a, b, A,$ and c states were found to be formed with quantum yields $\leq 0.0019, 0.4, 0.017, 0.000\ 15,$ and $0.000\ 61,$ respectively. Relative rotational and vibrational populations were measured for all states except for $\text{NH}(X)$. Average translational energies were estimated for $\text{NH}(a, v = 0 \text{ and } 1)$ and $\text{NH}(b, v = 0)$. The 248 nm photolysis of HN_3 was reinvestigated with respect to processes forming NH radicals other than $\text{NH}(a)$. The observed energy distributions differ for both laser wavelengths and for high and low lying NH states. The distribution can be better described by a simple impulsive than by a statistical model. Some conclusions are drawn concerning the upper HN_3 potential surfaces involved.

INTRODUCTION

Hydrazoic acid, HN_3 , is a fragile molecule. Its bond energy relative to formation of ground state $\text{NH}(X)$ and $\text{N}_2(X)$ is very small ($4000\ \text{cm}^{-1}$) and a number of different dissociation channels is accessible in the UV photolysis as displayed in Table I.

In previous work, one (or sometimes two) of the possible primary photolysis products have been directly observed.⁵⁻²³ In several of these studies, details on the internal energy distributions of the fragments have been obtained.^{6-8,10-13,17,20,20-22} It is generally believed that $\text{NH}(a)$ is the dominant primary product with a quantum yield near one.^{5,7-12} Excited $\text{NH}(A)$ ^{15,16,20} and $\text{NH}_2(\tilde{A})$ ^{8,9,22} radicals are noteworthy secondary products which can be efficiently generated in the HN_3 photolysis system even at low pressures.

It has been previously suggested in an UV photolysis study by Baronavski *et al.*⁸ that the dynamics of the photodissociation processes occurs by curve crossings or avoided curve crossings with predissociative bond levels. These authors (and also Tokue and Ito²⁴) have therefore recommended to study the branching ratios of the primary processes, particularly at higher excitation energies than previously used. The expectation was that such a study could lead to the construction of a complete potential energy diagram for this unimolecular reaction.⁸

Taking up this suggestion, we have chosen the excimer laser wavelengths of 193 nm (ArF) and 248 nm (KrF) to photolyze HN_3 at the bulk phase temperature of 300 K with the objective to give a detailed picture of all dissociation processes yielding the NH radical. In particular, the internal energy distributions of the different NH fragments and—where possible—their translational energies were studied. In addition, we report rough estimates of quantum yields for the formation of all NH states. The ArF excimer laser photolysis of HN_3 has been studied in our laboratory for some time¹⁷⁻²⁰ and the formation of $\text{NH}(a),$ ¹⁹ $\text{NH}(b),$ ¹⁸ $\text{NH}(A),$ ^{17,20} and $\text{NH}(c)$ ^{17,20} has been reported. So far, these

reports¹⁷⁻²⁰ give only a few details on the internal energy distributions of these photolysis fragments; their major aim was the investigation of kinetic properties of the excited NH states. Recently, the detailed energy distribution of $\text{NH}(a)$ formed in the 248 nm photolysis was investigated in our laboratory in connection with the formation of $\text{NH}(a)$ in the ammonia photolysis at 193 nm.²¹ The results of that study²¹ and those of the present investigation will be used here to give a detailed description of five out of seven possible photodissociation channels at 193 nm and on two of six channels at 248 nm.

EXPERIMENTAL

The NH photofragments, which were generated in the HN_3 photolysis, were detected either by their emissions or by laser induced fluorescences (LIF). Several features of the emission measurements have been reported previously.¹⁷⁻²⁰ Therefore, this technique will be described briefly. The method of detection by LIF will be described in more detail.

The same excimer laser (Lambda Physik, EMG 100) was used to generate KrF ($\lambda = 248\ \text{nm}; 200\text{--}250\ \text{mJ}$) or ArF ($\lambda = 193.3\ \text{nm}; 50\text{--}100\ \text{mJ}$) laser light. The unfocused photolysis laser beam had a cross section of $2.5\ \text{cm}^2$ as it entered the photolysis cell through a Suprasil window. In some experiments, dielectric filters were used to attenuate the fluence of the beam. The intensity of the KrF laser was observed to fluctuate less than that of the ArF laser and as a consequence the data taken for 248 nm were more precise. Any decrease in the intensity of the photolysis laser with time of operation was taken into account and the values of T_{rot} determined from different branches (which were measured at different times) were the same.

Emissions from excited NH states were detected at right angles to the excimer laser beam. Low resolution emission spectra of the highly forbidden $\text{NH}(b \rightarrow X)$ and $\text{NH}(a \rightarrow X)$ transitions were obtained at about 471¹⁸ and 794 nm.¹⁹ Excess of Ar was always present in these cases to minimize diffusion of the metastables from the photolysis volume. The $\text{NH}(b)$ state emission was also measured using a 0.5 m monochromator (Minuteman 305 M) at a resolution of $\Delta\lambda = 0.4\ \text{nm}$. The same monochromator was used to regis-

^{a)} Present address: Institut für Chemie 3: Atmosphärische Chemie der KFA Jülich, D-5170 Jülich, West Germany.

TABLE I. Products, dissociation energies, and threshold wavelengths for the photolysis of HN_3 .

Reaction	Products	Dissociation energy/cm ⁻¹ ^a	Threshold wavelength/nm
(1)	$\text{NH}(X) + \text{N}_2(X)^b$	4 000	2500
(2)	$\text{NH}(a) + \text{N}_2(X)$	16 590	603
(3)	$\text{NH}(b) + \text{N}_2(X)$	25 240	396
(4)	$\text{H}(^2S) + \text{N}_3(^2\Pi_g)$	31 060	322
(5)	$\text{N}(^4S) + \text{H}(^2S) + \text{N}_2(X)^b$	31 750	315
(6)	$\text{NH}(A) + \text{N}_2(X)^b$	33 780	296
(7)	$\text{NH}(c) + \text{N}_2(X)$	47 350	211
(8)	$\text{NH}(X) + \text{N}_2(A)$	53 760	186

The energies of KrF and ArF laser light correspond to 40 320 and 51 730 cm⁻¹, respectively.

^aThe dissociation energies are given for the products in their lowest vibrational and rotational states. The values for the heats of formation used for the calculation of the dissociation energies were taken from Ref. 1 for H and N, from Ref. 2 for NH, and from Ref. 3 for HN_3 and N_3 . The excitation energies were obtained from Ref. 4.

^bThe formation of these products violates spin conservation.

ter the spectra for the $\text{NH}(c \rightarrow a)$ and $\text{NH}(A \rightarrow X)$ transitions²⁰ with resolutions between 0.05 and 0.4 nm depending on intensity. A gated integrator (PAR 162/165) with a gate width of usually 1 μs accepted the signal from the photomultiplier. The same integrator was used to handle the signal in the LIF experiments.

The absolute efficiency of the detection system (0.5 m monochromator and photomultiplier) was determined using a calibrated D_2 lamp (UV 40; Optronic Laboratories) in the wavelength range 310–370 nm. The efficiency of detecting a photon emitted from the photolysis volume, ΔV , was estimated to be 5.3×10^{-7} assuming an isotropic distribution for the emission. To calculate the absolute number of $\text{NH}(c, v' = 0)$ produced, decay curves of the $\text{NH}(c, v' = 0 \rightarrow a, v'' = 0)$ band intensity were recorded with a transient recorder (Biomation 8100), then integrated to obtain the total intensity and compared with the signal measured for a single photon. The number of photons this way registered for a laser shot and the detection efficiency of a photon were then used to calculate the total emission intensity (number of photons emitted per laser shot).

For the LIF detection method, the excimer laser beam was crossed at right angles by a dye laser beam (Lambda Physik, FL 3002 pumped by a XeCl excimer laser, EMG 101). The dye laser beam originally had a cross section of 0.07 cm² but was expanded by a lens to about 18 cm² when intersecting the excimer laser beam. By this expansion and losses due to the lens, the original fluence of the dye laser was estimated to be reduced by a factor of about 500. All laser light pulses were about 15 ns long. The delay of the probing dye laser was controlled manually by a digitally selectable delay unit. The dyes used for pumping the singlet $\text{NH}(a$ and $b)$ and the triplet $\text{NH}(X)$ states are listed in Table II. During two experiments, LIF intensities of rotational lines in different dye ranges were compared. Therefore, the dye had to be exchanged which took about 1 min. The energies of all laser emissions were monitored by power meters (Gentec ED 200 and 500).

The fluorescence generated by the dye laser was detected perpendicular to the plane given by the excimer and dye laser beams. The fluorescence light was dispersed by a 0.2 m monochromator (Jobin Yvon H20) with the exit slit re-

TABLE II. Dyes and ranges of laser wavelengths used for the LIF detection. The energies and linewidths of the laser output and the NH transitions pumped are also given. The fluorescence emissions detected were those from the transitions $\text{NH}(A, v' = 0 \rightarrow X, v'' = 0)$ for all triplet and $\text{NH}(c, v' = 0 \rightarrow a, v'' = 0)$ for all singlet states.

Dye ^a	Wavelength /nm	Typical laser energy/mJ ^b	Linewidth /cm ⁻¹ ^c $\Delta\nu_L$	NH transition pumped
Sulforhodamin 101 (frequency doubled)	323–330	0.5	0.47 (at 325 nm)	$c, v' = 0 \leftarrow a, v'' = 0$
<i>p</i> -Terphenyl	332–350	3		$A, v' = 0 \leftarrow X, v'' = 0$
Butyl PBD	356–385	25	0.35 (at 363 nm)	$c, v' = 0 \leftarrow a, v'' = 1$
PBBO	386–420	8		$c, v' = 0 \leftarrow a, v'' = 2$
Coumarin 47	440–484	30	0.37 (at 452 nm)	$c, v' = 0 \leftarrow b, v'' = 0$
Coumarin 307	479–553	20		$c, v' = 0 \leftarrow b, v'' = 1$

^aTrade names as sold by Lambda Physik.

^bMeasured before expansion of the laser beam.

^cMeasured by using the Doppler widths of rotational lines at 300 K; the linewidths stated by the manufacturer (Lambda Physik) usually are slightly smaller.

moved. This resulted in a resolution of 30 nm. For the two LIF emissions observed, the monochromator was set to 326 nm to monitor emission from the $\text{NH}(c, v' = 0 \rightarrow a, v'' = 0)$ transition and to 336 nm for the $\text{NH}(A, v' = 0 \rightarrow X, v'' = 0)$ transition. With this spectral arrangement, all singlet and all triplet emission lines were received with equal weight. The boxcar integrator gate and the firing of the dye laser were slaved together. Usually for the LIF measurements, the gate was 500 ns wide and opened 20 ns after firing of the dye laser. This way, stray light from the probing dye laser was avoided but most of the fluorescence signal was collected. The output signal of the boxcar was simultaneously directed to a chart recorder and to an AD converter (Keithley 160 B) to be stored and processed by a computer (Zenith Z 100). The chart recorder traces were used to determine the widths of the laser lines listed in Table II (in the presence of 6650 Pa Ar and 0.65 Pa HN_3 , and at the long delay time of 20 μs) and the widths of the absorption lines.

Hydrazoic acid was prepared, stored, handled with great care, and used as described earlier.^{19,26} For the determinations of the laser line widths and the number of photons used in the generation of $\text{NH}(A)$ by KrF laser light, Ar was used as diluent gas which had the stated (Messer-Griesheim) minimum purity of 99.999%. Pressures in the photolysis cell were measured using capacitance manometers (MKS, Baratron, Type 222 A). Typically, 0.65 Pa HN_3 was photolyzed in the experiments with LIF detection. When monitoring direct emission, pressures ranging from 0.25 to 6.6 Pa HN_3 were used. Unless otherwise stated, the pressures used were sufficiently low to avoid quenching and relaxation. Ar was added in the 1.3 to 13.3 kPa range. For this purpose, Ar and HN_3 were premixed before use.

DATA ANALYSIS

Fluorescence spectra

The measured fluorescence intensity, $I_{J'J''}^{\text{em}}$, of a rotational line of an electronic transition from a state J' having an initial population $N_{J'}$ to a lower state J'' , is given by

$$I_{J'J''}^{\text{em}} = C_1 \tilde{\nu}^3 N_{J'} [S_{J'J''} / (2J' + 1)] \times [A_r \tau] [\exp(-t_a/\tau) - \exp(-t_e/\tau)]. \quad (1)$$

This equation represents a special application of formulas for emission intensities given in the literature²⁷ to the present detection method. C_1 and the C_i 's in the following equations are constants mainly representing the detection efficiency and $\tilde{\nu}$ is the wave number of the emission. The Hönl-London factors $S_{J'J''}$ were calculated according to known equations.²⁷ $A_r \tau$ represents the fraction of the population decaying by the monitored transition. $\tau = (\Sigma A_r + A_p + A_q)^{-1}$ is the measured fluorescence lifetime which is given by the sum of all radiative transition probabilities of the upper vibronic state (ΣA_r), the predissociation rate (A_p), and the quenching rate (A_q) of the emitting state J' . (For most of the present fluorescence spectra, $A_q \ll A_r$, since the pressures were sufficiently low.) For emissions from $\text{NH}(c, v' = 0)$, the values of $A_r(J')$ and $A_p(J')$ were taken from literature values.^{28,29} The last factor in Eq. (1) considers the position of the gate of the integrator, which opens and closes at times t_a and t_e , respectively, after the firing of the photolysis laser.

If $N_{J'}$ is given by a Boltzmann distribution, it is useful to modify Eq. (1) to give

$$I_{J'J''}^{\text{em}} / f_{J'J''}^{\text{em}} = C_1 N_{J'} / (2J' + 1) = C_2 \exp(-F_{J'} / kT_{\text{rot}}), \quad (2)$$

where $F_{J'}$ is the rotational energy of state J' ; T_{rot} is the rotational temperature, and $f_{J'J''}^{\text{em}}$ is given by

$$f_{J'J''}^{\text{em}} = \tilde{\nu}^3 S_{J'J''} A_r \tau [\exp(-t_a/\tau) - \exp(-t_e/\tau)]. \quad (3)$$

To obtain the relative vibrational population, we have used Eq. (2) and summed over J' for a given v' :

$$\sum_{J'} \{ (2J' + 1) I_{J'J''}^{\text{em}} / f_{J'J''}^{\text{em}} \} = C_1 \sum_{J'} N_{J'} = C_1 N_{v'}. \quad (4)$$

When determining the values of $f_{J'J''}^{\text{em}}$ for the relative vibrational population, we had to consider that τ can be different for the vibrational states [for example, the $\text{NH}(c, v' = 0)$ lifetime being affected by quenching in these experiments and the $\text{NH}(c, v'' = 1)$ lifetime by predissociation].

Laser induced fluorescence (LIF)

In LIF experiments using strong laser radiation fields, stimulated emission has to be taken into account. In LIF measurements, its contribution can lead to saturation effects. Cordova³⁰ has previously used a three level system to model the LIF intensity, $I_{J'J''}^{\text{LIF}}$, in dependence on the energy density in the laser field per unit frequency ρ . The equation he has derived is very useful, since it considers nonradiative processes such as quenching and predissociation and experimental parameters such as duration of the laser pulse t_L (taken to be of rectangular temporal width) and the gate position of the integrator (from t_a to t_e after the dye laser pulse). We have applied Cordova's equation, which has been previously used to evaluate LIF data,^{31,32} to conform to our experimental conditions such as short probe laser pulse duration, $t_L = 15$ ns, and t_a sufficiently large ($t_a \geq 15$ ns) to separate excitation from subsequent fluorescence. This way, the simplified equation for $I_{J'J''}^{\text{LIF}}$ is given by

$$I_{J'J''}^{\text{LIF}} = C_3 B_1 \rho [N_{J'} / (\lambda_2 - \lambda_1)] (\tau A_r) \exp(t_L/\tau) \times [\exp(-\lambda_1 t_L) - \exp(-\lambda_2 t_L)] \times [\exp(-t_a/\tau) - \exp(-t_e/\tau)]. \quad (5)$$

$N_{J'}$ is the population of the probed lower rotational state J'' , C_3 is the photon detection efficiency, and B_1 the Einstein coefficient for absorption. Predissociation of, for example, $\text{NH}(c, v' = 0)$ ^{28,29} has to be considered since $\tau = f(A_p)$.

The values of λ_1 and λ_2 in Eq. (5) are given by

$$\lambda_{1,2} = (1/2) [(B_1 + B_2)\rho + \tau^{-1}] \pm (1/2) \{ [(B_1 + B_2)\rho + \tau^{-1}]^2 - 4B_1\rho(\tau^{-1} - A_r) \}^{1/2}, \quad (6)$$

where

$$B_2 = g_1 B_1 / g_2 = c^3 S_{J'J''} A_r / [8\pi h \tilde{\nu}^3 (2J'' + 1)] \quad (7)$$

is the Einstein coefficient for stimulated emission and g_i represents the degeneracies of the respective states. Values of B_2 and B_1 were calculated by using values of $S_{J'J''}$ ²⁷ and A_r .^{28,29}

If a rotational temperature represents the distribution, Eq. (5) can be written to give

$$\begin{aligned} I_{J'J''}^{\text{LIF}}/f_{J'J''}^{\text{LIF}} &= C_3 N_{J''}/(2J'' + 1) \\ &= C_4 \exp(-F_{J''}/kT_{\text{rot}}), \end{aligned} \quad (8)$$

where

$$\begin{aligned} f_{J'J''}^{\text{LIF}} &= (S_{J'J''} A_r/\bar{v}^3) [\rho/(\lambda_2 - \lambda_1)] (\tau A_r) \exp(t_L/\tau) \\ &\quad \times [\exp(-\lambda_1 t_L) - \exp(-\lambda_2 t_L)] \\ &\quad \times [\exp(-t_a/\tau) - \exp(-t_e/\tau)]. \end{aligned} \quad (9)$$

The value of ρ was estimated as described below.

For low values of ρ , Eq. (5) results in

$$\begin{aligned} I_{J'J''}^{\text{LIF}} &= C_5 B_{J''} \rho \tau A_r N_{J''} t_L \\ &\quad \times [\exp(-t_a/\tau) - \exp(-t_e/\tau)] \end{aligned} \quad (10)$$

representing a linear relationship between $I_{J'J''}^{\text{LIF}}$ and ρ . At the given experimental conditions such as $\rho \bar{v}^3 \approx \text{const}$ and for $A_r = \text{const}$, Eq. (10) can be modified to yield

$$\begin{aligned} I_{J'J''}^{\text{LIF}}/S_{J'J''} & \\ &= C_6 N_{J''}/(2J'' + 1) = C_7 \exp(-F_{J''}/kT_{\text{rot}}) \end{aligned} \quad (11)$$

in case of a Boltzmann distribution. This equation is often used for the analysis of LIF data. In fact, the very first preliminary experiments in our laboratory when using the unexpanded dye laser beam to probe NH($a, v'' = 0, J''$) in the ArF laser photolysis of ammonia²¹ [though all reported data were taken with the expanded beam and applying an equation similar to Eq. (10)²¹] were evaluated this conventional way. Figure 1 shows, as an example, a plot of $\ln(I_{J'J''}^{\text{LIF}}/S_{J'J''})$ vs $F_{J''}$ from an initial spectrum described as an observation in Ref. 21. This figure clearly demonstrates, that the population $N_{J''}/(2J'' + 1)$ depends on the branch evaluated, with the R branch pretending a population being about 2.6 times that represented by the other branches. It should be noted that the separate analysis of all three branches agree reasonably well on the rotational temperature. A similar result has been recently observed for OH(X).³² As shown in Fig. 1 by the full data points, the inconsistency in the population is removed by using $\rho = 1.02 \times 10^{-10} \text{ J s m}^{-3}$ which was obtained with ρ as a parameter in Eq. (8) and (9). [This value was found to yield equal values of $I_{J'J''}^{\text{LIF}}/f_{J'J''}^{\text{LIF}}$ for the R(3) and Q(3) lines, the line strengths of which are different by as much as a factor of

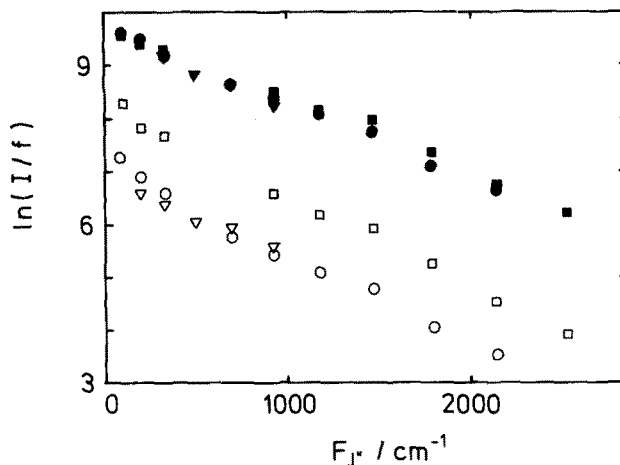


FIG. 1. Relative population of NH($a, v'' = 0, J''$), $N_{J''}/(2J'' + 1) \propto I/f$, from the LIF intensities of the NH($c, v' = 0 \leftarrow a, v'' = 0$) transition as a function of the rotational energy $F_{J''}$. Measurements with the unexpanded dye laser beam. For $I/f = I_{J'J''}^{\text{LIF}}/S_{J'J''}$: \square , R-branch line; \circ , Q-branch line; ∇ , P-branch line intensities. For $I/f = I_{J'J''}^{\text{LIF}}/f_{J'J''}^{\text{LIF}}$, the respective full symbols, $\blacksquare, \bullet, \blacktriangledown$, represent the data (see the text). The NH(a) radicals were generated in the photolysis of 6.5 Pa ammonia using an ArF laser of 60 mJ (Ref. 21). The delay between excimer and dye laser was 2 μs .

4.] The calculations furthermore show, that, within the error limits, a linear dependence of $I_{J'J''}^{\text{LIF}}$ on ρ [Eq. (10)] is given for a reduction in ρ by no less than a factor of 10. As done previously in our laboratory,²¹ the dye laser fluence was reduced by about a factor of 500. Although the linear relationship (10) hence is justified, we have used Eqs. (8) and (9) for the determination of the rotational distributions. In several experiments relative values of ρ were needed. For this purpose, the value of ρ was estimated by assuming it to be linearly and inversely proportional to the dye laser fluence and bandwidth, respectively, at constant laser light pulse duration. This way, we obtained a value of $\rho = 2.1 \times 10^{-10} \text{ J s m}^{-3}$ for the unexpanded beam which is in reasonable agreement with the value of ρ given above.

The relative population of two vibrational states was estimated by comparing the intensities of two rotational lines, $I_{J'J''}^{\text{LIF}}(v'')$, each from a different vibrational level v'' . The ratio of population of two vibrational states such as the NH($a, v'' = 1$ and 0) states, $N_{v''=1}/N_{v''=0}$, then is obtained from

$$\begin{aligned} & [I_{J'J''}^{\text{LIF}}(v'' = 1)/f_{J'J''}^{\text{rot}}(v'' = 1)] / [I_{J'J''}^{\text{LIF}}(v'' = 0)/f_{J'J''}^{\text{rot}}(v'' = 0)] \\ &= [N_{v''=1}/N_{v''=0}] [B_1(v'' = 1)\rho(v'' = 1)f^{\text{gate}}(v'' = 1)] / [B_1(v'' = 0)\rho(v'' = 0)f^{\text{gate}}(v'' = 0)]. \end{aligned} \quad (12)$$

Equation (12) is based on Eq. (10) with the fraction of the vibrational population represented by the rotational line intensity given by

$$f_{J'J''}^{\text{rot}}(v'') = (2J'' + 1) \exp(-F_{J''}/kT_{\text{rot}}) / Q_{\text{rot}} \quad (13)$$

(Q_{rot} is the rotational partition function). The value of

$$f^{\text{gate}}(v'') = (\tau A_r) [\exp(-t_a/\tau) - \exp(-t_e/\tau)] \quad (14)$$

essentially is the correction for the gate position and predisociation.

While values of $A_r(J')$ are given in the literature for the ($c, v' = 0 \leftarrow a, v'' = 0$) transition,^{28,29} the corresponding values for the ($c, v' = 0 \leftarrow a, v'' = 1$ and $b, v'' = 0$) transitions are not known and were estimated in the present work from relative transition probabilities³³ scaled with the J dependence given by Smith and Hsu²⁸ for the ($c, v' = 0 \leftarrow a, v'' = 0$) transition. Because of lacking data, we have assumed the absolute value

of $A_r(c, v' = 1 - a, v'' = 0)$ to be equal to $0.19 \times A_r(c, v' = 0 - a, v'' = 0)$. The factor of 0.19 considers the different Franck-Condon factors.³³ Moreover, the fluorescence lifetimes of $\text{NH}(c, v' = 1, J')$ have been previously²⁹ observed to be almost constant for low J' (which are dominantly populated in this work). We hence adopted A_r to be independent of J' in this case. The relative rotational population in $N_{J'}(v' = 1)$ is then mainly determined by $I_{J', J''}^{cm}(v' = 1)/S_{J', J''}$. In order to guess a value for the unknown probability of the $\text{NH}(c, v' = 0 - b, v'' = 1)$ transitions, we have assumed the relative transition probabilities of the $(c - b)$ system to be the same as those of the $(c - a)$ system. Furthermore, no values of A_r are known for the $(c, v' = 0 - b, v'' = 1$ and $a, v'' = 2)$ transitions and upper limits for the population of these vibrational a and b state levels will not be given in this work.

Absorption of laser light

For an estimate of the quantum yield, we need to know the number of NH radicals formed and the number of photons absorbed. Intense laser beams such as those of unfocused excimer lasers often are barely attenuated while photolyzing a large fraction of the molecules traversed. For a laser with constant intensity during its pulse time, t_L , and having a spacially uniform intensity profile, the number of photons lost by absorption, Δn_p , in the photolysis volume, ΔV , is given by

$$-\Delta n_p / \Delta V = -\Delta N = N_a - N_e \\ = N_a [1 - \exp(-\sigma n_p / A)], \quad (15)$$

where N_a and N_e are the concentrations of the photolyzed species before and after the laser pulse, respectively; σ is the absorption cross section, which can be obtained as described below, and A the cross section of the laser beam; n_p is the number of the laser photons of the light pulse. For a photodissociation process requiring the absorption of one photon, ΔN represents the concentration of the dissociated parent molecules.

The number of laser photons, $n_{p,e}$, left after passing an absorbing layer of length d is calculated to be

$$n_{p,e} = (A/\sigma) \ln \{ [\exp(\sigma n_{p,a}/A) - 1] \\ \times \exp(-N_a \sigma d) + 1 \}. \quad (16)$$

For $N_a = 0, n_{p,e} = n_{p,a}$ with $n_{p,a}$ being the number of photons entering the system. Equation (16) allows one to determine the effective absorption cross section for the laser light.

RESULTS

Upon irradiation of HN_3 with ArF excimer laser light, emissions from the following allowed NH transitions were observed: $(c, v' = 0 \rightarrow a, v'' = 0$ and $1)$; $(c, v' = 1 \rightarrow a, v'' = 0)$; $(c, v' = 0 \rightarrow b, v'' = 0)$, $(A, v' = 0 \rightarrow X, v'' = 0$ and $1)$; $(A, v' = 1 \rightarrow X, v'' = 0$ and $1)$. [It should be noted that the $(c, v' = 1 \rightarrow a, v'' = 1)$ transition was not observed and did not interfere with the $(c, v' = 0 \rightarrow a, v'' = 0)$ emission, because of the short lifetime of $v' = 1$ and the delayed gate position used to monitor $v' = 0$.] As an example, Fig. 2 shows the spectrum measured for the $\text{NH}(c, v' = 0 \rightarrow b, v'' = 0)$ transition being about 30 times

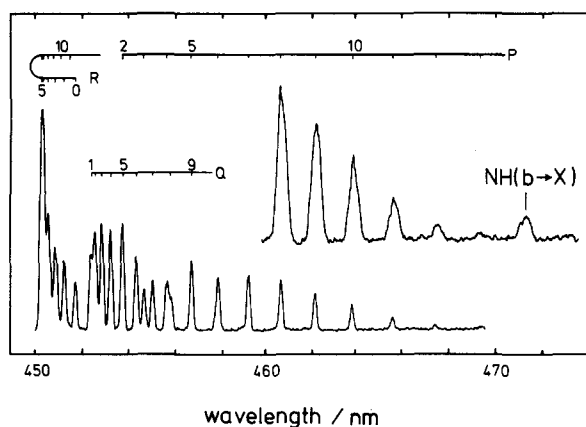


FIG. 2. Spectrum of the $\text{NH}(c, v' = 0 \rightarrow b, v'' = 0)$ emission. The inset shows rotational lines for higher values of J' and the $\text{NH}(b \rightarrow X)$ emission. HN_3 at 4.25 Pa was photolyzed by ArF laser irradiation at 60 mJ. Gate width: 500 ns, delay 20 ns; spectral resolution 0.15 and 0.38 nm for the inset.

weaker than the competing $(c, v' = 0 \rightarrow a, v'' = 0)$ transition.³³ This figure additionally exhibits the weak Q branch of the forbidden $\text{NH}(b, v' = 0 \rightarrow X, v'' = 0)$ transition. In separate experiments, several weak rotational lines of the highly forbidden $(a, v' = 0 \rightarrow X, v'' = 0)$ transition were detected in the ArF laser photolysis.¹⁹ Unfortunately, the emissions from both the metastable $\text{NH}(a$ and $b)$ fragments had to be obtained under experimental conditions (high pressures of inert gas and wide gates) not allowing the original rotational, vibrational, and translational energy distribution to be measured. Since the original energy distribution was an aim of our investigation, LIF measurements were performed on these slowly decaying states at low total pressures and short delays after the photolysis laser pulse to obtain the desired information.

Besides the previously reported formation of $\text{NH}(a, v = 0$ and $1)$ ²¹ the only other detected NH state in the KrF laser photolysis was $(A, v' = 0)$ the emission of which was extremely weak; in particular, no $\text{NH}(b$ and $X)$ could be detected. As the data in Table I shows, $\text{NH}(c)$ cannot be formed with 248 nm light.

Fluence dependence

The number of photons, n , absorbed for the formation of an NH radical was determined for each fluorescence and laser induced fluorescence emission monitored in the present work except for the $\text{NH}(A, v' = 1 \rightarrow X, v'' = 1)$ fluorescence which was too weak at the low pressures of HN_3 necessary. For this purpose, the logarithm of the fluorescence intensities, I_F , was plotted vs the logarithm of the laser intensities, I_L , according to equation $I_F = C \times I_L^n$ where C is a constant. I_L was varied by at least a factor of 10 in the case of ArF laser and by at least a factor of 7 in the case of KrF laser photolysis. The value for n was obtained to be $1.0 \pm 0.1 (3\sigma)$ for all emissions reported here. The triplet $\text{NH}(A, v' = 0 \rightarrow X, v'' = 0)$ fluorescence yielded a value of $n \approx 1$ only at sufficiently low pressures of HN_3 ($P < 0.3$ Pa). At higher pressures a value close to two was measured. This result is in agreement with a previous measurement¹⁷ and

indicates secondary reactions which generate additional NH(*A*). These reactions could apparently be suppressed in the KrF laser photolysis of up to 10 Pa HN₃ when large amounts of Ar were added.

Population distribution in the NH(*c*) and NH(*A*) states

From the observed emission spectra, relative populations in the different rotational, vibrational, and Λ states were deduced. For the NH(*c*, $v' = 0$ and 1) states, rotational populations $N_{J'}$ for quanta up to $J' = 11$ could be registered. Pressures of HN₃ ranging from 0.27 to 6.7 Pa were used but no change in the rotational spectrum was observed for NH(*c*, $v' = 0$) in this pressure range. This indicates effective freezing of the rotational distribution in accord with the corresponding large quenching constant $(8.50 \pm 0.32) \times 10^{-10} \text{ cm}^3 \text{ s}^{-1}$.³⁴ The rotational populations of the NH(*c*, $v' = 0$ and 1) states were evaluated using Eq. (2). Figure 3 displays the values of $N_{J'}/(2J'+1) \propto I_{J'J'}^{\text{em}}/f_{J'J'}^{\text{em}}$ in a semilogarithmic plot vs the energy of the rotational state $F_{J'}$. This figure shows that the population slightly deviates from a Boltzmann distribution. A regression fit to all data (full line) results in a rotational temperature $T_{\text{rot}} = 750 \pm 130 \text{ K}$ (3σ). This value agrees with that determined before in our laboratory ($T_{\text{rot}} = 700 \text{ K}$).¹⁷ When simulating singlet spectra at low resolution, a rotational temperature of 810 K was found to be more appropriate. This value is represented in Fig. 3 by the dashed line which clearly emphasizes low rotational levels.

Because, for the (*c* → *a*) emission, the (0,0) band overlaps with the (1,1) band, the (1,0) band at 305 nm was used to determine the rotational population in NH(*c*, $v' = 1$). It should be noted, that, according to published Franck-Condon factors,³³ the (1,1), (1,0), and (1,2) bands are expected to exhibit similar intensities, but the (1,2) band was not observed in the present work. The results of the evaluation of

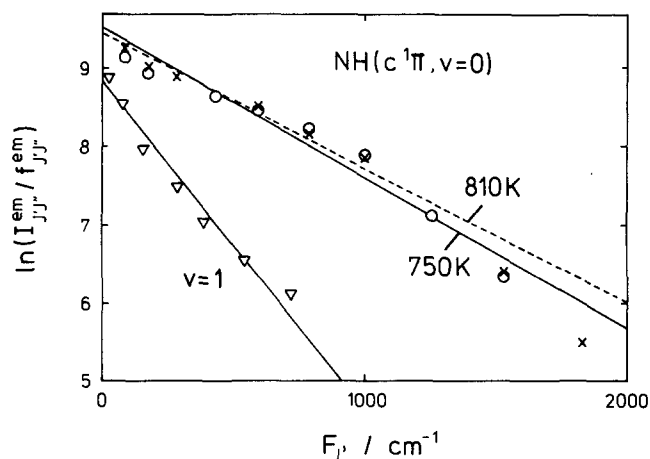


FIG. 3. Rotational population $N_{J'}/(2J'+1) \propto I_{J'J'}^{\text{em}}/f_{J'J'}^{\text{em}}$ of NH(*c*, $v = 0$ and 1) in the ArF laser photolysis of HN₃ as a function of the rotational energy $F_{J'}$. For $v = 0$ the *Q*-line data (*x*) and *P*-line data (*o*) and for $v = 1$ the *P*-line data (∇) are presented. The full line for $v = 0$ is a regression fit to all data points ($T_{\text{rot}} = 750 \text{ K}$). The dashed line emphasizes data at low J' and represents $T_{\text{rot}} = 810 \text{ K}$. The regression fit to the data for $v = 1$ yields $T_{\text{rot}} = 350 \text{ K}$.

the intensities of the *P*(2) to *P*(8) lines of the (1,0) band is displayed in Fig. 3 and represented by a distribution well approximated by the rotational temperature $T_{\text{rot}} = 350 \pm 100 \text{ K}$. The relative vibrational population of the NH(*c*, $v = 0$ and 1) states was obtained by Eq. (4) yielding 95% of the population in $v = 0$ and 5% in $v = 1$.

The relative population of the two Λ components of the NH (*c*¹ Π) state cannot be deduced from the strong NH(*c* → *a*) emission since the corresponding emission lines are too closely spaced ($\Delta\lambda \approx 0.01 \text{ nm}$) for the present resolution. The NH(*c* → *b*) transition (Fig. 2), however, allows one to monitor the different Λ components by the *Q*- and *R*-, *P*-branch emissions. No difference (within $\pm 20\%$) in the population of the two Λ states were observed.

In order to completely suppress secondary formation of NH(*A*), triplet NH(*A* → *X*) emission spectra were taken for HN₃ pressures not exceeding 0.3 Pa which were hence limited to a spectral resolution of 0.4 or 0.2 nm. At this low resolution, single rotational lines could not be resolved. The rotational and the vibrational populations in the NH(*A*) state were therefore estimated by simulation of the spectra as described recently.²⁰ This way, a rotational distribution corresponding to $T_{\text{rot}} = 3000 \pm 500 \text{ K}$ was estimated. At higher pressures of HN₃, secondary reactions become noticeable and at 6.7 Pa HN₃, for example, T_{rot} was determined to be 4000 K while the number of photons absorbed to generate this NH(*A* → *X*) emissions was found to be significantly greater than one. It should be noted that the dominant feature determining the rotational temperature was the envelope of the *P* branch since the *R* branch is overlapped by the singlet emission and the *Q* branch does not show any structure at the resolution used. The rotational distribution in the vibrationally excited NH(*A*, $v = 1$) state was roughly estimated to be represented by a value of T_{rot} between 500 and 2000 K. Since also for the triplet emission, the (1,1) band is heavily overlapped by the (0,0) band, a more accurate value cannot be given here. From the simulations, it was estimated that 86% of the NH(*A*) populate $v = 0$ and 14% $v = 1$.

The relative population of the different Λ components of the NH(*A*³ Π , $v = 0$) state can be monitored by the relative intensities of the *Q* and the *P*, *R* branches. No preference for one Λ state was observed contrary to the population of the components of the NH(*A*, $v = 0$) radicals formed in the ArF laser photolysis of NH₂(\tilde{X}^2B_1)³⁵ radicals.

The NH(*A* → *X*) emission intensity observed in the KrF-laser photolysis was too small to be evaluated. The data of this section and the following data obtained by LIF are summarized in Table III.

Population distribution in NH(*X*, *a*, *b*)

Since the *c* and *A* states were already formed as primary photolysis products in the ArF laser photolysis, a delay of about seven lifetimes ($\sim 3 \mu\text{s}$) had to be applied before LIF measurements were performed. Since no NH(*c*) emission is produced in the KrF laser photolysis, the delay was $1 \mu\text{s}$. The relative rotational population, $N_{J'}$, of the NH(*a*, $v = 0$ and 1) and NH(*b*, $v = 0$) states were calculated from intensity measurements by use of Eq. (8). The highest rotational quanta J'' detected for the singlet NH(*a*, *b*) states was deter-

TABLE III. Summary of the experimental results obtained for the rotational temperature, T_{rot} ; fraction of vibrational excitation, $N(v)/N$; translational energy, E_{trans} ; and quantum yield, ϕ , for the given electronic NH product states.

Product state	v	T_{rot}/K	$N(v)/N$	$E_{\text{trans}}/\text{cm}^{-1}$ ^a	ϕ
ArF excimer laser					
NH(X)	0				<0.002
NH(a)	0	3150 ± 750	0.79	26 200	0.40
	1	2450 ± 380	0.21	23 700	
NH(b)	0	1510 ± 350	> 0.95	19 800	0.02
NH(A)	0	3000 ± 500	0.86		0.0002
	1	~ 1000	0.14		
NH(c)	0	810 ± 100	0.95		0.0006
	1	350 ± 100	~ 0.05		
KrF excimer laser ^b					
NH(a)	0	1180 ± 150	0.58	10 600	1 ^c
	1	1140 ± 120	0.42	11 300	
NH(A)	0				very small

The given error limits represent three times the standard deviation.

^a $E_{\text{trans}} = kT_{\text{trans}}$.

^b The data was taken from Ref. 21 and was reevaluated for this work.

^c Value assumed to be 1 for NH(a).

mined by the strong predissociation of $\text{NH}(c, v=0)$ for $J' > 17^{29}$. Figure 4 shows an example of a spectrum obtained by pumping different rotational levels of the $\text{NH}(a, v=0)$ state. Figure 5 exhibits the corresponding values of $N_{J'}/(2J'+1) \propto I_{J'J''}^{\text{LIF}}/f_{J'J''}^{\text{LIF}}$ in a logarithmic plot vs $F_{J'}$. From plots like those shown in this figure, rotational temperatures $T_{\text{rot}} = 3150 \pm 750$ K and 2450 ± 380 K were deduced in the ArF laser photolysis for $\text{NH}(a, v=0)$ and 1), respectively.

For $J' \geq 7$, absorption lines from different Λ components of the $\text{NH}(a^1\Delta)$ state could be resolved ($\Delta\lambda \approx 0.061$ nm, due to the splitting in the c state), but no difference in

their population was detected at the time of detection ($3 \mu\text{s}$ after their generation) as the insert of Fig. 4 [$P(15)$ lines of ($c \leftarrow a$) transition] confirms.

The relative vibrational distribution of the $\text{NH}(a, v=0)$ and 1) states was estimated by measuring the intensities of two rotational lines: one Λ component of the $P(15)$ lines of the (0,0) band at 335.743 nm and both unresolved Λ components of the $Q(2)$ line of the (0,1) band at 362.750 nm. [The Λ degeneracy of the $Q(2)$ line was taken into account for the intensity ratios.] During this experiment, the dyes had to be exchanged. The LIF intensities were evaluated according to Eq. (12) to obtain values for $N_{v'=1}/N_{v'=0}$. The intensities of the $P(15)$ and $Q(2)$ lines were found to decrease very quickly ($\tau \approx 5 \mu\text{s}$) according to first order, although the

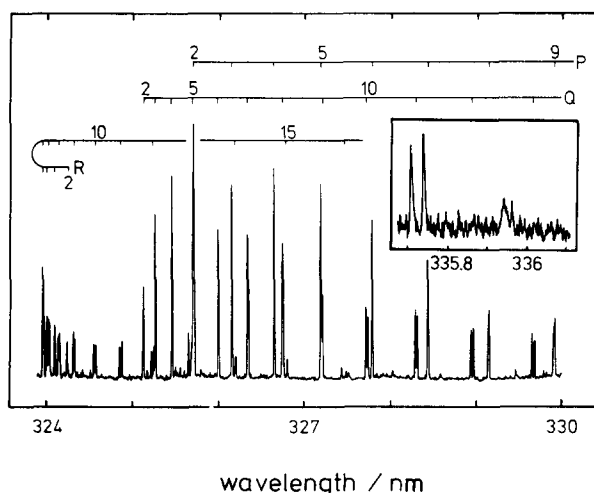


FIG. 4. LIF spectrum of the $\text{NH}(c^1\Pi, v'=0 \leftarrow a^1\Delta, v''=0)$ transition in the ArF laser photolysis of 0.65 Pa HN_3 . The dye laser was delayed by $3 \mu\text{s}$; the boxcar gate was $0.5 \mu\text{s}$, delay $0.1 \mu\text{s}$. The insert shows the $P(15)$ lines of the $\text{NH}(c \leftarrow a)$ transition and weakly the Q branch of the $\text{NH}(A, v=0 \leftarrow X, v=0)$ transition near 335.9 nm.

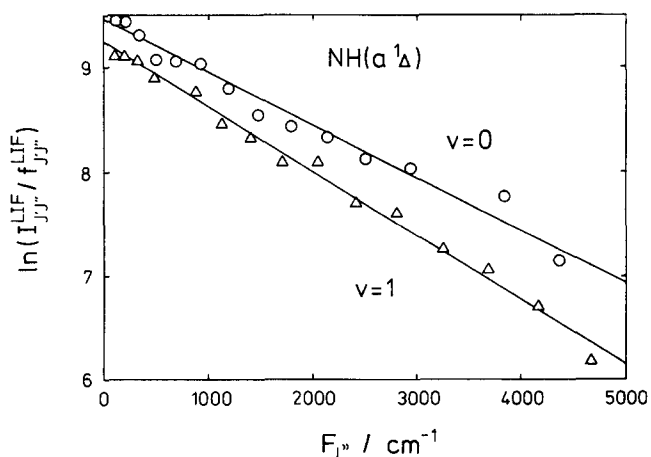


FIG. 5. Rotational population $N_{J'}/(2J'+1) \propto I_{J'J''}^{\text{LIF}}/f_{J'J''}^{\text{LIF}}$ of $\text{NH}(a, v=0)$ and 1) in the ArF laser photolysis of HN_3 as a function of the rotational energy $F_{J'}$. The lines represent $T_{\text{rot}} = 3150 \pm 750$ K for $v=0$ and 2450 ± 380 K for $v=1$.

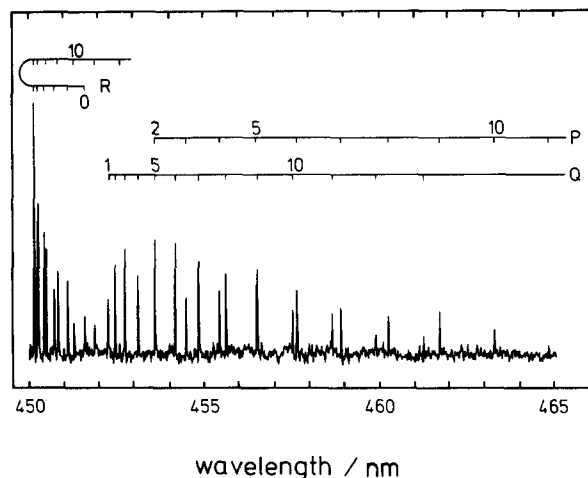


FIG. 6. LIF spectrum of the NH($c, v' = 0 \leftarrow b, v'' = 0$) transition in the ArF laser photolysis of HN₃ at 0.65 Pa. The dye laser was delayed by 3 μ s; the boxcar gate was 0.5 μ s, and the delay 0.1 μ s.

pressure was low (0.65 Pa HN₃) to minimize collisions. The decaying intensities were therefore extrapolated to time zero when the photolysis laser was fired. With this extrapolation, we obtain the result that 79% of the NH(a) is formed in $v = 0$ and 21% in $v = 1$. Vibrationally excited NH($a, v'' = 2$) radicals were searched for but were not detected in this work possibly because of low detection sensitivity.

One of the two LIF spectra recorded for NH($b, v'' = 0$) is shown in Fig. 6. The corresponding distribution of the rotational population is displayed in Fig. 7. This distribution is remarkable for its relatively low population of $J'' = 0$ and 1. The rotationless state possesses only half of the population predicted by the Boltzmann distribution given in Fig. 7 by the straight line. A slight inversion is indicated in this case. Apart from this, the rotational temperature appears to be given by $T_{\text{rot}} = 1580 \pm 550$ and 1470 ± 400 K for the two recorded spectra. Table III lists the weighted average of both measurements. The search for NH($b, v = 1$) was unsuccessful as well as the search for NH($b, v = 0$) in the KrF laser photolysis.

Translational energies of NH(a and b)

Linewidths for the absorbing NH(a, b) radicals were determined by LIF as done recently in our laboratory with the same dye laser system.²¹ The linewidths were measured at 0.65 Pa for different delay times. It was observed that the widths decreased with time. Therefore, the measured linewidths were extrapolated to time zero, their time of generation, using a first order time dependence. This dependence was chosen, since it represents the changes of the widths measured in the extensively studied KrF laser photolysis at 1, 3, 5, 7, and 9 μ s delay particularly well.

All evaluated line shapes could be well approximated by Gauss functions. The experimentally observed linewidth, $\Delta\nu_{\text{expt}}$, was hence used to yield Doppler linewidths, $\Delta\nu_D$, according to $\Delta\nu_{\text{expt}}^2 = \Delta\nu_L^2 + \Delta\nu_D^2$.³⁶ The values of $\Delta\nu_D$ were used to calculate the average translational energies,

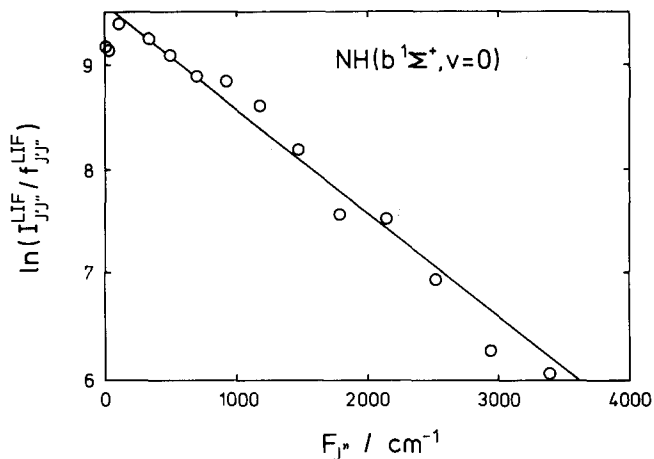


FIG. 7. Rotational population $N_{J''} / (2J'' + 1) \propto I_{J''}^{\text{LIF}} / f_{J''}^{\text{LIF}}$ of NH($b, v = 0$) in the ArF laser photolysis of HN₃ vs rotational energy $F_{J''}$. The line represents $T_{\text{rot}} = 1580 \pm 550$ K.

E_{trans} , of the NH radicals. The resulting values of E_{trans} are given for NH(a, b) in Table III. For the purpose of comparison, Table III (and Table IV) additionally lists the results recently obtained in our laboratory in the KrF laser photolysis of HN₃ by Kenner *et al.*²¹ To be consistent, the original data of Ref. 21 were reevaluated in this work according to the present procedure which resulted in insignificant changes for the values of the rotational and small changes in the vibrational and translational distributions.

Quantum yields

The absolute value of the quantum yield was calculated in this work only for the primary production of NH($c, v = 0$) by ArF laser photolysis. By comparison of

TABLE IV. Energy distribution for the different degrees of freedom. The internal energies, E_{rot} , E_{vib} , and E_{trans} are referred to the available energy, E_{avl} . The experimental data are those from Table III.^a

Product state	v	$E_{\text{avl}}/\text{cm}^{-1}$	$\frac{E_{\text{rot}}}{E_{\text{avl}}}$	$\frac{E_{\text{vib}}}{E_{\text{avl}}}$	$\frac{E_{\text{trans}}}{E_{\text{avl}}}$
ArF excimer laser					
NH(X)	0	47 730			
NH(a)	0	35 140	0.062		0.74
	1	31 960	0.053	0.019	0.74
NH(b)	0	26 490	0.040	<0.006	0.75
NH(A)	0	17 950	0.12		
	1	14 940	~0.05	0.024	
NH(c)	0	4 380	0.13		
	1	2 270	0.11	~0.024	
KrF excimer laser					
NH(a)	0	23 730	0.035		0.45
	1	20 550	0.039	0.057	0.55
NH(A)	0	6 540			

^a $E_{\text{trans}} = kT_{\text{trans}}$; $E_{\text{rot}} = kT_{\text{rot}}$; $E_{\text{vib}} = \sum_v (N_v [G(v) - G(v=0)]) / N$; $E_{\text{avl}} = E_{\text{hv}} - \Delta H_0^0 - G(v) + G(v=0)$, where $G(v)$ is the vibrational energy of state v ; the values of E_{hv} and the dissociation energies, ΔH_0^0 , were taken from Table I.

emission intensities, the quantum yields were obtained for $\text{NH}(A)$ and $\text{NH}(b)$. The yield for $\text{NH}(a)$ was estimated by relative LIF intensities from $\text{NH}(a)$ and $\text{NH}(b)$. The same quantum yield at 193 nm was additionally determined in comparison with its yield in the KrF laser photolysis. Finally, the yield for the primary production of $\text{NH}(X)$ was estimated relative to that for $\text{NH}(a)$ by LIF intensity measurements. The quantum yield of $\text{NH}(A)$ at 248 nm was observed to be very small and was not measured.

To estimate the absolute quantum yield for $\text{NH}(c, v' = 0)$, $\phi(c, v' = 0)$, first the number of photons emitted from the photolysis volume, $\Delta V = 3.7 \text{ cm}^3$, was estimated. This number had to be corrected for the fraction of the emission lines monitored (48%) and the excited radicals lost by predissociation (34%). Small corrections were included for the competing $(c, v' = 0 \rightarrow b)$ (3.3%) and $(c, v' = 0 \rightarrow a, v'' = 1)$ transitions (4.6%). In this experiment, a pressure of 0.13 Pa HN_3 was used and the ArF laser energy was 28 mJ. For these conditions, we calculate that 1.82×10^9 $\text{NH}(c, v' = 0)$ radicals were formed. Then the absorption cross section was determined for 193 nm using Eq. (16). Values of $n_{p,e}$ were measured as a function of N_a and fitted to Eq. (16) with the help of the simplex method.³⁷ This way, the value of σ at 193.3 nm was determined to be $2.8 \times 10^{-18} \text{ cm}^2$ which compares well with that previously reported by Okabe ($\sigma = 2.4 \times 10^{-18} \text{ cm}^2$).¹⁶ Using this value of $\sigma(193 \text{ nm})$ and Eq. (15), we found that 3.14×10^{12} laser photons were absorbed in ΔV (i.e., 2.7% of the HN_3 molecules were photolyzed) and hence $\phi(c, v' = 0) = 5.8 \times 10^{-4}$. When the vibrationally excited radicals are included $\phi(c) = 6.1 \times 10^{-4}$ is obtained. This value of $\phi(c)$ is in good agreement with the value given by Okabe¹⁶ at 184.9 nm [$\phi(c) < 7 \times 10^{-4}$].

As recently described,²⁰ the quantum yield for the $\text{NH}(A)$ radicals was obtained by comparing the total $(A, v' = 0 \rightarrow X, v'' = 0)$ intensity with that of the $(c, v' = 0 \rightarrow a, v'' = 0)$ band. This was performed by first simulating the spectra and then evaluating the ratio of the intensities according to Eq. (4). In addition to the processes considered in our recent work,²⁰ we have included predissociation of $\text{NH}(c, v = 0)$ and its competing emission channels leading to $\text{NH}(b)$ and $\text{NH}(a, v = 1)$ and obtain $\phi(A) = 0.25 \phi(c)$ and, hence, $\phi(A) = 0.00015$.

As evident from Fig. 2, the Q branch of the forbidden $\text{NH}(b, v' = 0 \rightarrow X, v'' = 0)$ transition appears next to the $\text{NH}(c, v' = 0 \rightarrow b, v'' = 0)$ emission. At 4.25 Pa HN_3 , quenching of $\text{NH}(c, v = 0)$ had to be taken into account for the determination of $\phi(b)$. Similar to $\text{NH}(a)$, the $\text{NH}(b)$ radicals were found to have an effective lifetime ($\tau \approx 3 \mu\text{s}$, determined by LIF) in the observed volume, which is very much shorter than their radiative lifetime, $\tau_{\text{rad}} = 97 \text{ ms}$.³⁸ Considering a large correction by the ratio of the radiative and measured lifetimes and taking into account the transition probability of $\text{NH}(c, v' = 0 \rightarrow b, v' = 0)$,³³ and the fact that the Q branch of the $\text{NH}(b, v' = 0 \rightarrow X, v'' = 0)$ transition represents half of the total emission, we calculate $\phi(b) = 0.017$.

For the determination of $\phi(a)$, the LIF intensity of a $P(15)$ line of the $\text{NH}(c, v = 0 \rightarrow a, v = 0)$ transition at

335.743 nm (Fig. 4) was compared with that of the $Q(6)$ lines of the $\text{NH}(c, v = 0 \rightarrow b, v = 0)$ transition at 454.224 nm (Fig. 6). This method is very similar to that used to obtain the relative vibrational population of $\text{NH}(a)$. The measured intensities and the corrections according to Eq. (12) resulted in a value $\phi(a, v' = 0) = 0.31$. With the vibrational excitation of $v = 1$ included, $\phi(a) = 0.4$.

Figure 4 shows that the Q branch of the $(A, v = 0 \rightarrow X, v = 0)$ lies close to the $P(15)$ lines of the $\text{NH}(c, v = 0 \rightarrow a, v = 0)$ band. The Q branch represents half of the total triplet LIF intensity. The fraction of $\phi(a, v = 0)$ represented by a $P(15)$ line was calculated as before [Eq. (12)]. This way, the very weak triplet signal results in a value of $\phi(X) < 0.002$. No triplet LIF signal was observed in the KrF laser photolysis.

Because of accumulation of possible errors during the procedure of estimation and due to the lack of reliable data on the relevant transition probabilities, the value of $\phi(a)$ given above is not expected to be very accurate. To confirm the estimate, we have compared the yields of $\text{NH}(a, v = 0)$ at the photolysis wavelengths of 248 and 193 nm. In this experiment, the different laser intensities, the HN_3 absorption cross sections, and the fractions of the total band represented by the monitoring $Q(2)$ line of the $(c, v = 0 \rightarrow a, v = 0)$ transitions (T_{rot} is different for both photolysis wavelengths) had to be taken into account. Assuming $\phi(a, v = 0)$ at 248 nm is 0.58 (Table III), and using Eq. (12), we obtain $\phi(a) = 0.38$, which we estimate to be accurate within $\pm 70\%$. The major uncertainty in this measurement is the value for the absorption cross section of HN_3 at 248 nm, which was not determined in the present work. Following the procedure described previously,²¹ we have adopted $\sigma(248 \text{ nm})$ to be $6.9 \times 10^{-20} \text{ cm}^2$ and believe that this value is accurate within $\pm 40\%$. It should be noted that in this experiment the LIF detection system stayed unchanged while the excimer laser wavelength was changed.

DISCUSSION

In this work, we have obtained information about five of the seven energetically possible dissociation channels for HN_3 (see Table I). This makes hydrazoic acid one of the few small molecules for which a large number of competing channels have been identified. In this section, we first discuss limitations and uncertainties of the results given in Tables III and IV, which displays the energy data of Table III in relation to the energy available in the respective photodissociation process. Then we compare our results with those of previous authors. This will be followed by a comparison of our results with two simple models, the statistical and the impulsive model. Finally, we discuss the data obtained at various wavelengths on the basis of the knowledge available for electronically excited HN_3 states.

Although most of the data of Tables III and IV were determined with reasonable precision, one should be aware of a number of limitations restricting their accuracy. One major obstacle consisted in unknown or barely known values for transition probabilities, A_r , for the following transitions as mentioned in an earlier section: $(c, v' = 0 \rightarrow a, v'' > 1)$ and

$b, v'' > 0$), $(c, v' = 1 - a, v'')$, and $(c, v' = 0, J' - a, v'' = 1, J''$ and $b, v'' = 0, J''$), respectively. Consequently, we cannot exclude, that $\text{NH}(a, v > 1)$ and $\text{NH}(b, v > 0)$ radicals are formed in this photolysis system.

Another serious limitation is the LIF detection of the lower X , a , and b states after delays of at least $3 \mu\text{s}$ (and $1 \mu\text{s}$ when using the KrF laser). The measured average kinetic energies correspond to an $\text{NH}(a, b)$ velocity of about $0.6 \text{ cm } \mu\text{s}^{-1}$ which can easily explain the short residence times of these radicals in the probed volume. For the determination of the vibrational distributions and Doppler widths, we have therefore extrapolated the measured data to time zero. This, however, was not done for the rotational populations since it would have required very extensive experimental work. If the escaped radicals carried a significantly different rotational distribution than that measured, their absence during the time of probing would introduce an error in the given rotational distribution. The large velocity also increases the probability of collisions during the delay time although low pressure of HN_3 (0.65 Pa) was used. These collisions might have introduced some relaxation mainly for the rotational and translational energy distribution.

The measured fractions of the available energy appearing in the translational motion of $\text{NH}(a, b)$ in the ArF laser photolysis ($E_{\text{trans}}/E_{\text{avl}} = 0.74$) seem to be slightly too large in terms of conservation of energy and momentum. While temperatures represent the overall distribution of the rotational population reasonably well (see Figs. 3, 5, and 7), it is doubtful whether a temperature describes the distribution of the translational energy. For a photolysis process occurring on a steeply repulsive potential surface, by far the most of the excess energy will be channeled into translation as described later by the impulsive model. Consequently, the energy distribution could be sharply peaked around large values of E_{trans} . We have furthermore assumed an isotropic distribution of the photofragment trajectories which may not be justified as the photolysis system is anisotropic [and produces polarized emission from $\text{NH}(c)$ ³⁹]. Although a simulation of the shape of the $R(11)$ doublet lines of the $(c, v' = 0 \leftarrow a, v'' = 0)$ LIF transition by Gauss functions yielded good agreement with the measured line profiles at $3 \mu\text{s}$ delay, it is doubtful, whether the line shape is purely Gaussian. How much the relatively wide laser line shape masks the true line shape was not investigated in this work and, in particular, no such elaborate method as, for example, velocity aligned Doppler spectroscopy⁴⁰ was used.

The values of ϕ for the various dissociation channels (see Table III) exhibit large differences of up to a factor of 3×10^3 . Because of the relative evaluation procedure, the absolute values of the quantum yields become less accurate for $\text{NH}(c, A, b, a, X)$ in the given order. We estimate the value of $\phi(c)$ to be accurate within $\pm 20\%$. We were unable to directly estimate the uncertainties in the remaining values of quantum yields due to the complex evaluation procedure and the uncertainties in the estimated transition probabilities. However, we have confirmed the value of $\phi(a) = 0.4$, which is the only significant quantum yield in this work, by an independent measurement as described above. This second determination mainly relies on the quantum yield

$\phi(a, v = 0)$ at 248 nm which was taken to be $1 - \phi(a, v = 1) = 0.58$ (Table III) and the value of $\sigma(248 \text{ nm})$. Both $\text{NH}(a, v = 0$ and $1)$ are formed in the 248 nm photolysis with almost equal efficiency.²¹ It is hard to accept that $v = 2$ is not formed at all. Moreover, no absolute value of $\phi(a, 248 \text{ nm})$ has been reported yet. Therefore, $\phi(a, v = 0, 248 \text{ nm}) \leq 0.58$ should be taken as an upper limit and $\phi(a, 193 \text{ nm}) \leq (0.38 \pm 0.24)$, i.e., the present work only accounts for about half of the photolysis products.

The low value for $\phi(a, 193 \text{ nm})$ implies, that additional photolysis processes occur, which we are not able to detect, such as $\text{NH}(a, v > 1$ and $b, v > 0)$ and reactions (4) and (5) of Table I. The spin forbidden reaction (5) escapes our detection method, although we can estimate that 34% of the initially formed $\text{NH}(c, v = 0$ and $1)$ will finally yield $\text{N} + \text{H} + \text{N}_2$ via predissociation at collisionless conditions. The formation of $\text{H} + \text{N}_3$ [reaction (4)] has been previously reported to occur in the quartz UV¹⁴ and with a quantum yield of 0.03 – 0.05 at 213.9 nm .²⁵ A low quantum yield for the production of $\text{H} + \text{N}_3$ is in agreement with a previous theoretical study⁴¹ and can certainly not explain the missing photolysis process.

Because of the uncertainties described above, error limits are given in Table III only for the rotational temperatures, which are represented in each case by a number of line intensities.

Besides some preliminary studies from this laboratory,^{17–20} the only other investigation known to us at 193 nm is that of Hall *et al.*¹³ who observed the $\text{NH}(a)$ vibrational fundamental. These authors report a very high rotational temperature of $10200 \pm 800 \text{ K}$ for $\text{NH}(a, v = 0)$ and a translational temperature of $570 \pm 60 \text{ K}$ based on IR absorption scans over the $R(14)$ and $R(25)$ lines several μs after the ArF laser pulse in HN_3 at 13 Pa . It should be noted for $T = 300 \text{ K}$, that the lifetime of $\text{NH}(a)$ is estimated to be about $0.3 \mu\text{s}$ at $13 \text{ Pa } \text{HN}_3$.¹⁹ An induction period was observed and the high rotational temperature most likely is due to secondary processes.¹³ Vibrational excitation was not observed in that work although the authors cannot exclude its possibility.

The KrF laser (248 nm) photolysis of HN_3 has been discussed in some detail in recent work from this laboratory.²¹ In agreement with previous work,¹⁰ no ground state $\text{NH}(X)$ was observed. The most surprising result is the efficient generation of $\text{NH}(a, v = 1)$ radicals in both the 248^{21} and 193 nm photolysis, a result that is in variance with earlier investigations at 248 nm .^{10,12} It has been noted previously^{21,42} that, under the conditions employed in the earlier work,¹⁰ it would not have been possible to detect $\text{NH}(a, v > 0)$ because of predissociation of $\text{NH}(c, v > 0)$. It is interesting to note that previously vibrationally excited $\text{NH}(a, v > 0)$ radicals have been observed in flash photolysis experiments^{6,7} and were proposed to explain the formation of stable products in the 213.9 nm photolysis of HN_3 .²⁵

The most extensive UV photolysis study has been performed by McDonald and co-workers^{8,11,22} using 266 nm irradiation by a quadrupled Nd:YAG laser. The only fragment detected was $\text{NH}(a, v = 0)$ and its quantum yield $\phi(a, v = 0, 266 \text{ nm})$ has therefore been reported to be one.^{8,22}

These results now appear to be suspect in the light of previous comments on the detection of $\text{NH}(a, \nu > 0)^{21,42}$ and should be checked. No indications for the generation of $\text{NH}(b, X, \text{ and } A)$ radicals have been observed in their work. The rotational temperature of the $\text{NH}(a, \nu = 0)$ radicals was determined to be 1207 ± 26 K which is close to the value of previous work (1180 ± 150 K)²¹ from our laboratory at 248 nm and the present reevaluation in Table III. This is fortuitous, since those authors did not correct for predissociation in the $\text{NH}(c, \nu = 0)$ state which was excited for their LIF detection.^{8,22} They have estimated the upper limit of the translational energy to be 5200 cm^{-1} and have concluded from this energy partitioning that the other fragment, $\text{N}_2(X)$, must possess about $11\,000 \text{ cm}^{-1}$ tied up probably in vibrations.

Tables III and IV show that the translational energy and its fraction of the available energy markedly decrease with increasing wavelength. As we suggest below, this might be due to the different dissociation dynamics in the different absorption regions. Whether this decrease continues down to $E_{\text{trans}} = 5200 \text{ cm}^{-1}$ at 266 nm⁸ in the same (first) absorption region was not investigated in this work. On the other hand, we do not exclude that the translational energy given by Baronavski *et al.*⁸ might increase upon correction for rapidly escaping fast radicals.

In the following, we compare the energy distributions in the NH fragments with the predictions from two simple models: the statistical⁴³ and the impulsive model.^{44,45} Using the statistical model, the relative population for the rotational and vibrational degrees of freedom were calculated³⁴ simply by distributing the available energy without any other restriction. The very large fraction of the excess energy appearing in the translational mode already suggests that the statistical model most likely fails to predict the energy distribution. This was confirmed for the rotational levels which are calculated to carry about one fourth of the excess energy in contrast to the results displayed in Table IV. Substantial vibrational excitation is predicted, but the variation of the vibrational distributions displayed in Tables III and IV is not at all reflected by the statistical model. In particular, the trend of increased vibrational excitation of $\text{NH}(a)$ shown in Table III for longer photolysis wavelengths is not reproduced. We therefore conclude that none of the observed five dissociation processes is statistical.

The impulsive model was used in two ways.³⁴ First we have treated H–N–N₂ as an triatomic molecule having a stiff N₂ fragment bond during the repulsion of the two products.⁴⁴ Then, we have calculated the energy partitioning for the case that the excess energy is originally released in the motion of the two repellent N atoms, the bond of which is broken. This model assumes soft bonds⁴⁵ and allows compression of the fragment N₂ bond during the dissociation process resulting in vibrational excitation of the N₂ product. The HN_3 structure at the transition state was taken as given for the ground state⁴⁶ but the N–N–N angle was adopted to be 180° instead of 171.3° .⁴⁶ This small change is of minor importance to the energy distribution in the NH fragment.

The comparison of the predictions by this very simple model with the experimental data of Table IV³⁴ can be sum-

marized as follows: (a) The assumption of a stiff N₂ bond appears to be appropriate for the 193 nm and of a soft bond for the 248 nm photolysis. A soft N₂ bond results in significant vibrational excitation of the N₂ fragment and, as a consequence, yields noticeably smaller fractions of the excess energy for translation and rotation (see 248 nm photolysis in Table IV). (b) The fractions of translational energy are reasonably well represented by the impulsive model. (c) The predicted rotational energies are slightly smaller than the measured ones for the low lying $\text{NH}(a \text{ and } b)$ states, but a factor of about 3 smaller for the energetically higher $\text{NH}(A \text{ and } c)$ states. (d) The impulsive model predicts the vibrational energy to be 4 to 10 times too low. This discrepancy could be even greater in view of our possible inability to detect $\text{NH}(a, \nu > 1 \text{ and } b, \nu > 0)$ radicals and cannot be accounted for by the change of the NH bond length which is the same in the radical⁴ and ground state HN_3 .⁴⁶ Nonetheless, from the overall qualitative agreement, we suggest that the dissociation process is impulsive, i.e., it occurs on a repulsive curve. However, the simple description we are presenting here has to be refined to account for the large vibrational excitation in all NH states and for the large rotational excitation in the upper excited $\text{NH}(A \text{ and } c)$ states.

The qualitative comparison of the experimental data with the predictions from the impulsive model implies that the dissociation processes considered in this work occur via at least three different excited HN_3 states. The lowest of these states (excited by 248 nm light) yields $\text{NH}(a)$. At 193 nm, at least two more states are involved, one of which generates the products $\text{NH}(a \text{ and } b)$. The other one gives $\text{NH}(A)$ and $\text{NH}(c)$. The two HN_3 states leading to the formation of the metastables NH states at 193 and 248 nm have H–N–N equilibrium bond angles, which are not much different from that of the ground state. Hence, H–N–N bending will not induce marked rotation in the $\text{NH}(a)$ and $\text{NH}(b)$ states. On the other hand, the third state leading to $\text{NH}(A \text{ and } c)$ is proposed to have a bent H–N–N structure, which is considerably different from that of the ground state. This way, the relatively large rotational population in the upper triplet and singlet NH states can be justified by an excited HN_3 state, which intends to relax to its angular equilibrium, while it dissociates. Similarly, the rotational excitation in $\text{NH}(a)$ from the photolysis of HNCO has been explained recently.⁴⁷

The HN_3 absorption spectrum and its analysis⁴⁸ largely support the implications mentioned above. The first, second, and third absorption region exhibit maxima at about 270, 205, and 190 nm, respectively.⁴⁸ At 193 nm, both the second and third absorption region overlap. Both first and second absorption region exhibit weak diffusive vibrational structure. Besides bending, antisymmetric stretch in the first and symmetric stretch vibration in the second region has been identified for the N–N–N frame.⁴⁸ According to the impulsive model, the N–N–N bending motion can barely induce significant rotation in the NH fragment (contrary to a previous suggestion⁴¹), but will directly influence rotation of the N₂ fragment, which was not monitored in the present work. A similar concept has been recently developed to explain the rotational excitation of CO in the photolysis of

HNCO.⁴⁹ In a simple picture, stretching vibrations appear to be more efficient for the dissociation than bending motions. In the antisymmetric stretch mode, the fragment N₂ bond is compressed while the broken HN–N₂ bond length is increased. In the symmetric mode, there is a synchronous movement of both atoms in the N₂ fragment away from the NH fragment. These opposite or synchronous movements in the departing N₂ fragment might justify the assumption of soft and stiff bonds in the 248 and 193 nm photolysis, respectively.

The SCF-CI study by Sevin *et al.*⁴¹ indicates that minima of the excited HN₃ potentials are reached for vertical excitation. During elongation of the HN–N₂ bond, the excited state molecule has to overcome a barrier. Moreover, the structures in the first two absorption regions are indicative for excitation of bond states which are predissociative.⁸ The bond states have severely elongated N–N bond lengths.⁴⁸ It appears to be reasonable to assume that the energies of the resulting symmetric and antisymmetric stretch vibrations couple into the vibration of the N–H bond during the short lifetime of the excited HN₃ state. This might be the reason that we find the vibrational distribution closer to that predicted by the statistical than to that given by the impulsive model. In MO description, the N–H bond length might be differently affected during the breaking of the HN–N₂ bond depending on the involvement of orbitals of *a'* or *a''* symmetry in the excitation process. However, this has to await clarification by further theoretical work.

In conclusion, many features of this extensive experimental description of the photodissociation of HN₃ at two wavelengths can be qualitatively explained. Most likely, the dissociation process is complex and crossings and avoided crossings of potential surfaces are involved. For example, a previously reported correlation diagram correlates the first excited ¹A' (¹Δ) state directly with NH(*c*).²⁴ The excitation of a ¹A' state was confirmed by polarization experiments to form NH(*c*),³⁹ but the yield of NH(*c*) was measured to be very low. To fully understand the dynamics of the simultaneous formation of all five NH fragments, additional, theoretical work appears to be necessary.

ACKNOWLEDGMENTS

We thank Dr. R. D. Kenner and Professor V. Staemmler for many discussions during the course of this work, R. K. Browarzik for the results on polarization, and Professor J. C. Kinsey for sending us the relevant parts of the theses of Dr. J. F. Cordova and Dr. J. A. Silver. Financial support by the Deutsche Forschungsgemeinschaft (SFB 42) and Fonds der Chemischen Industrie is gratefully acknowledged.

¹M. W. Chase, Jr., J. L. Curnutt, J. R. Downey, Jr., R. A. McDonald, A. N. Syverud, and E. A. Valenzuela, *J. Phys. Chem. Ref. Data* **3**, 462 (1974).

²S. T. Gibson, J. P. Greene, and J. Berkowitz, *J. Chem. Phys.* **83**, 4319 (1985).

³C. F. Melius (private communication, 1986).

⁴K. P. Huber and G. Herzberg, *Molecular Spectra and Molecular Structure. IV. Constants of Diatomic Molecules* (Van Nostrand Reinhold, New York, 1979).

⁵H. Okabe, *Photochemistry of Small Molecules* (Wiley, New York, 1978).

⁶R. J. Paur and E. J. Bair, *J. Photochem.* **1**, 255 (1972/73).

⁷R. J. Paur and E. J. Bair, *Int. J. Chem. Kinet.* **8**, 139 (1976).

⁸A. P. Baronavski, R. G. Miller, and J. R. McDonald, *Chem. Phys.* **30**, 119 (1978).

⁹L. G. Piper, R. H. Krech, and R. L. Taylor, *J. Chem. Phys.* **73**, 791 (1980).

¹⁰B. M. Dekoven and A. P. Baronavski, *Chem. Phys. Lett.* **86**, 392 (1982).

¹¹J. W. Cox, H. H. Nelson, and J. R. McDonald, *Chem. Phys.* **96**, 175 (1985).

¹²W. Hack, Habilitationsschrift, Universität Göttingen 1986.

¹³J. L. Hall, H. Adams, J. V. V. Kasper, R. F. Curl, and F. K. Tittel, *J. Opt. Soc. Am. B* **2**, 781 (1985).

¹⁴D. E. Milligan and M. E. Jacox, *J. Chem. Phys.* **41**, 2838 (1964).

¹⁵K. H. Welge, *J. Chem. Phys.* **45**, 4373 (1966).

¹⁶H. Okabe, *J. Chem. Phys.* **49**, 2726 (1968).

¹⁷H. K. Haak and F. Stuhl, *J. Phys. Chem.* **88**, 3627 (1984).

¹⁸U. Blumenstein, F. Rohrer, and F. Stuhl, *Chem. Phys. Lett.* **107**, 347 (1984).

¹⁹F. Rohrer and F. Stuhl, *Chem. Phys. Lett.* **111**, 234 (1984).

²⁰F. Rohrer and F. Stuhl, *J. Chem. Phys.* **86**, 226 (1987).

²¹R. D. Kenner, F. Rohrer, and F. Stuhl, *J. Chem. Phys.* **86**, 2036 (1987).

²²J. R. McDonald, R. G. Miller, and A. P. Baronavski, *Chem. Phys. Lett.* **51**, 57 (1977).

²³H. Esser, J. Langen, and U. Schurath, *Ber. Bunsenges. Phys. Chem.* **87**, 636 (1983).

²⁴I. Tokue and Y. Ito, *Chem. Phys.* **79**, 383 (1983).

²⁵R. S. Konar, S. Matsumoto, and B. deB Darwent, *Trans. Faraday Soc.* **67**, 1698 (1971).

²⁶G. Pannetier and F. Margineanu, *Bull. Soc. Chim.* **7**, 2617 (1972).

²⁷G. Herzberg, *Molecular Spectra and Molecular Structure. I. Diatomic Molecules* (Van Nostrand Reinhold, New York, 1950).

²⁸W. H. Smith and D. K. Hsu, *J. Quant. Spectrosc. Radiat. Transfer* **22**, 223 (1979).

²⁹W. H. Smith, J. Brzozowski, and P. Erman, *J. Chem. Phys.* **64**, 4628 (1976).

³⁰J. F. Cordova, Ph.D. dissertation, MIT, Cambridge, 1980.

³¹J. F. Cordova, C. T. Rettner, and J. L. Kinsey, *J. Chem. Phys.* **75**, 2742 (1981).

³²S. Zabarnick, J. W. Fleming, and A. P. Baronavski, *J. Chem. Phys.* **85**, 3395 (1986).

³³J. M. Lents, *J. Quant. Spectrosc. Radiat. Transfer* **13**, 297 (1973).

³⁴F. Rohrer, Dissertation, Ruhr-Universität Bochum, 1987.

³⁵R. D. Kenner, R. K. Browarzik, and F. Stuhl, *Chem. Phys.* (to be published).

³⁶R. Schmiedl, R. Böttner, H. Zacharias, U. Mier, and K. H. Welge, *Opt. Commun.* **31**, 329 (1979).

³⁷J. N. Demas, *Excited State Lifetime Measurements* (Academic, New York, 1983).

³⁸C. M. Marian and R. Klotz, *Chem. Phys.* **95**, 213 (1985).

³⁹R. K. Browarzik (unpublished results).

⁴⁰Z. Xu, B. Koplitz, and C. Wittig, *J. Chem. Phys.* **87**, 1062 (1987).

⁴¹A. Sevin, J. P. Le Roux, B. Bigot, and A. Devaquet, *Chem. Phys.* **45**, 305 (1980).

⁴²G. T. Fujimoto, M. E. Umstead, and M. C. Lin, *Chem. Phys.* **65**, 197 (1982).

⁴³(a) R. D. Levine and J. L. Kinsey, in *Atom-Molecule Collision Theory*, edited by R. B. Bernstein (Plenum, New York, 1979); (b) A. Ben-Shaul, Y. Haas, K. L. Kompa, and R. D. Levine, *Lasers and Chemical Change*, Springer Series in Chemical Physics Vol. 10 (Springer, Berlin, 1981).

⁴⁴G. E. Busch and K. R. Wilson, *J. Chem. Phys.* **56**, 3626 (1972).

⁴⁵A. F. Tuck, *J. Chem. Soc. Faraday Trans. 2* **73**, 689 (1977).

⁴⁶B. P. Winnewisser, *J. Mol. Spectrosc.* **82**, 220 (1980).

⁴⁷T. A. Spiglanin and D. W. Chandler, *J. Chem. Phys.* **87**, 1577 (1987).

⁴⁸J. R. McDonald, J. W. Rabalais, and S. P. McGlynn, *J. Chem. Phys.* **52**, 1332 (1970).

⁴⁹T. A. Spiglanin, R. A. Perry, and D. W. Chandler, *J. Chem. Phys.* **87**, 1568 (1987).